ELECTRO-OSMOTIC EFFECT ON PERISTALTIC FLOW OF PHAN–THIEN–TANNER FLUID IN A PLANAR CHANNEL

MAHADEV M. CHANNAKOTE[1], **SHEKAR M.**[2] and **V. K. DILIPKUMAR**[3]

Abstract

There are several factors that can cause the excessive accumulation of biofluid in human tissue, such as pregnancy, local traumas, allergic responses or the use of certain therapeutic medications. This study aims to further investigate the shear-dependent peristaltic flow of Phan–Thien–Tanner (PTT) fluid within a planar channel by incorporating the phenomenon of electro-osmosis. This research is driven by the potential biomedical applications of this knowledge. The non-Newtonian fluid features of the PTT fluid model are considered as physiological fluid in a symmetric planar channel. This study is significant, as it demonstrates that the chyme in the small intestine can be modelled as a PTT fluid. The governing equations for the flow of the ionic liquid, thermal radiation and heat transfer, along with the Poisson–Boltzmann equation within the electrical double layer, are discussed. The long-wavelength ($\delta \ll 1$) and low-Reynolds-number approximations ($Re \rightarrow 0$) are used to simplify the simultaneous equations. The solutions analyse the Debye electronic length parameter, Helmholtz–Smoluchowski velocity, Prandtl number and thermal radiation. Additionally, streamlines are used to examine the phenomenon of entrapment. Graphs are used to explain the influence of different parameters on the flow and temperature. The findings of the current model have practical implications in the design of microfluidic devices for different particle transport phenomena at the micro level. Additionally, the noteworthy results highlight the advantages of electro-osmosis in controlling both flow and heat transfer. Ultimately, our objective is to use these findings as a guide for the advancement of lab-on-a-chip systems.

[1]Department of Mathematics and Statistics, M. S. Ramaiah University of Applied Sciences, Bengaluru, Karnataka 560054, India; e-mail: mchannakote@rediffmail.com
[2]Department of Mathematics, B. M. S. College of Engineering, Bengaluru, Karnataka 560019, India; e-mail: shekarm872@gmail.com
[3]Department of Mathematics, Gurunanak Dev Engineering College, Bidar, Mailoor Road Bidar, Karanataka 585403, India; e-mail: dilipkalse@gmail.com

1. Introduction

Peristalsis is the term used to describe the rhythmic, wave-like movement of chyme through the small intestine. Conversely, segmentation refers to the contraction of circular smooth muscles, which causes pinching and aids in mechanical digestion. This process is responsible for the movement of fluid in a flexible tube. Peristalsis is one of the main physiological processes involved in fluid movement. It can be found in both animal and human bodies, facilitating the transport of urine from the kidney to the bladder, vasomotion in tiny blood vessels, the passage of chyme through the gastrointestinal system and the movement of sanitary fluids, among other functions. Latham, in 1966 [22], conducted a significant theoretical investigation on peristalsis, marking a milestone in understanding this phenomenon. Several studies have been reported on the peristaltic flow of both Newtonian and non-Newtonian fluids in different geometrical configurations [1, 3, 5, 23, 25, 27]. These recent contributions from various authors have greatly advanced our understanding of peristaltic transport, considering the impact of diverse physical features across different flow geometries.

Modern fluid mechanics has witnessed a significant growth in the field of electro-kinetic transfer. This area of study focuses on the interaction between electrolytic fluids and external electric fields, whether they are static or alternating. Researchers explore these phenomena through experimental methods and analysis, uncovering a range of intricate and captivating observations. These include the distribution of charges, behaviour of wetted surfaces, zeta potentials and electric double layers. Additionally, the field of electro-kinetics encompasses other phenomena such as electro-osmosis, electrophoresis and diffusiophoresis, which are particularly relevant when considering chemical gradients. Specifically, electro-osmosis occurs when a fluid flows, while a solid surface remains stationary in the presence of an electric field. This phenomenon is commonly observed in various diseases, cellular abnormalities, drug delivery test kits based on cells, sickle cell disease and other medical conditions. The electro-kinetic phenomena known as electro-osmotic flow or electro-osmosis were first described by Reuss [32] in 1809. It refers to the movement of fluid in a conduit, such as a capillary tube or microchannel, when a strong external electric field is applied. When a charged solid surface comes into contact with water or a watery solution, negative charges will appear on the surface. The positive ions in the liquid will then be attracted to the surface, while the negative ions will resist it. This creates a thin layer called the electrical double layer (EDL) with an imbalanced charge. When the electric field is parallel to the solid surface, the positively charged EDL will move in the direction of the electric field. Haung et al. [18] described the electro-osmotic flow in capillaries using a monitoring technique. Gravesen et al. [14] conducted a comprehensive review on the various applications of microfluidics. Haswell [15] focused on the progressive aspects of micro-flows in relation to electro-osmotic flow. There is now a wealth of literature available on electro-osmosis in different flow patterns [4, 20, 41].

In recent years, there has been significant growth in the mathematical modelling of electro-osmotic phenomena due to peristaltic activity. This growth is driven by the clinical and commercial synthesis of electro-osmotic devices, as simulation plays a crucial role in advancing this field. Chakraborty [9] was the first to elucidate the peristalsis phenomenon in electro-osmotic flow. Through this approach, investigations have made valuable contributions to our understanding of the peristaltic transport of non-Newtonian fluids in different fluid models [6, 13, 24, 33, 36, 37, 40]. The reliability of a non-Newtonian fluid model depends on the power or applied stress. Unlike Newtonian fluids, non-Newtonian fluids cannot be characterized by a single constant viscosity due to their complex nature. They can include liquid polymer ions, colours, blood and other polymer configurations. In these fluids, there is a nonlinear relationship between strain rate and shear pressure, which can be time-dependent. Consequently, it is not possible to establish a constant coefficient of thickness. Understanding the behaviour of non-Newtonian fluids is crucial in various mechanical and design processes, such as oil penetration, paper manufacture, glass blowing, plastic sheet development, food handling, formation of organic liquids, heat pipes, vapour distribution and active cooling.

For studying the rheological behaviour of fluids, the Pan–Thien–Tanner (PTT) liquid model is considered to be the most appropriate. The PTT liquid model is a unique model that demonstrates both shear thinning and viscoelasticity. The PTT constitutive equation accurately predicts the rheology of concentrated polymer solutions. Recent advancements have resulted in significant practical applications for studying peristaltic transport using PTT liquid in various geometrical shapes across multiple industries and physiological fields. This mechanism is used in the medical and physiological sectors to develop artificial heart-lung machines, and ensure the secure disposal of hazardous liquids by nuclear companies, among other applications. Abd El Naby [2] discussed the peristaltic propulsion of PTT fluid in creeping flow, considering the constraints of long wavelength. Hayat et al. [16] conducted an analysis on peristaltic activity in a planar channel using PTT fluid. Prakash and Tripathi [29] studied the flow of PTT fluid under the influence of peristalsis in an asymmetric channel. Vajravelu et al. [39] simulated peristaltic flow and heat transfer of a conductive PTT fluid in an asymmetric channel, mimicking the movement of chyme in the small intestine. Hussain et al. [19] examined the effects of the peripheral layer and electro-osmotic force on the peristaltic flow of the PTT fluid. Mahadev and Mohanta [23] explored the impact of thermal radiation on the PTT liquid model, considering peristaltic activity and cilia waves. Butt et al. [7] discussed the analysis of heat transfer in peristaltic flow caused by cilia's metachronal wave in a PTT fluid. Heat transfer has recently garnered attention due to its potential applications in physiology, engineering and business. Specifically, the flow of blood, heat conduction in tissue, convective heat conduction through blood movement within tissue and the diffusion of nutrients from the blood are all crucial components of peristaltic processes that rely on heat transmission. Relevant courses on heat transport in peristalsis include haemodialysis and oxygenation. In recent times, there has been extensive research on peristalsis with

heat transmission, and many of these studies are accessible. Channakote and Asha [10] examined the peristaltic motion of fractional second-grade fluid regulated by electro-osmosis. Rathod and Mahadev [31] discussed heat transfer in the peristaltic flow of fractional second-grade fluid. Channakote and Kalse [12] investigated the effects of convective and viscous dissipation on peristaltic flow of Ellis fluid in a nonuniform tube. They also [11] explored the peristaltic flow of Rabinowitsch fluid in a channel with a permeable wall under the influence of heat transfer. Several other notable studies in this area can be found in the literature [8, 26, 28, 34].

Radiation and conduction are the primary prerequisite mechanisms in the heat transfer process. Due to the pool of thermal radiation energy, which all matter accumulates and has a temperature of zero, thermal radiation is a powerful energy that is amplified by matter as magnetic waves. However, in certain situations, the amount of heat exchanged through radiation may be a very small fraction of the total, and therefore can be disregarded. The relative importance of different heat transport mechanisms varies greatly with temperature. Conduction and convectional heat transmission are primarily influenced by the temperature difference and are not significantly affected by the surrounding temperature. In contrast, radiation does not require an intermediary medium for heat transmission, unlike conduction and convection. The amount of thermal radiation emitted by a human body is influenced by its surface condition and temperature. When a body is heated, it emits radiant energy that extends slightly beyond the apparent range of wavelengths. This phenomenon has been studied in various applications such as nuclear power plants, boilers, engine cooling processes, and furnaces. Kothandapani and Prakash [21] discussed the effects of heat radiation on peristaltic transportation. Rafiq and Abbas [30] examined the impact of thermal radiation and viscous dissipation on the peristaltic flow of the Rabinowitsch viscoelastic fluid in a nonuniform inclined tube. Sunitha and Asha [35] investigated the influence of heat radiation on the peristaltic blood motion of a Jeffrey liquid containing double diffusion with gold nanoparticles. Hayat et al. [17] provided insights into the magneto nanofluid flow in a porous channel with the combination of radiative peristaltic flow and thermal radiation.

The aim of this study is to use the PTT fluid model in a two-dimensional symmetric channel with electro-osmotic phenomenon in peristalsis, inspired by the efficiency of the aforementioned effects. The study focuses on the effects of heat transfer and thermal radiation on peristaltic transport. It is important to note that the PTT liquid has consequences for shear thickening, shear thinning and time relaxation properties. The main focus of the study is to analyse the liquid rheology, Helmholtz–Smoluchowski velocity (U_{hs}) effects and Debye length effects in the complex flow structure. The resulting equations are quantitatively determined using MATHEMATICA software. The effects of various parameters on velocity, temperature, pressure rise and trapping phenomenon are discussed in the graph. This research has significant implications for lab-on-chip systems used for diagnostics, where fluids are studied and their transit may be stimulated by an external electric field. Electro-osmotic pumps provide high pressure and flow without the need for mechanical components. The model and

the obtained results are associated with the pumping phenomenon in organs and vessels.

2. Constitutive equations

The behaviour of an extra stress tensor for the linear PTT fluid model is (as seen in [16, 39])

$$T = -pI + \tau,$$

$$f(tr(\tau))\tau + K\tau^\nabla = 2\mu\mathbb{D},$$

$$\tau^\nabla = \frac{d\tau}{dt} - \tau.\mathbb{L}' - \mathbb{L}.\tau,$$

$$f(tr(\tau)) = 1 + \frac{\epsilon\kappa}{\mu}tr(\tau),$$

where $\mathbb{L} = \text{grad } V$.

In the above equations, p is the pressure, I is the identity tensor, μ is the dynamic viscosity, τ is the extra stress tensor, $\mathbb{D}$ is the deformation rate tensor, K is the relaxation time, τ^∇ denotes Oldroyds's upper convected derivative, d/dt is the material time derivative, tr is the trace, V is the velocity vector and prime indicates the transpose. It is significant to note that when the extensional parameter is zero, the PTT model simplifies to an upper convicted Maxwell model.

3. Mathematical formulation

The geometric model of the electro-osmotic peristaltic flow of incompressible viscoelastic fluid in the current study is illustrated in Figure 1. We choose the electro-osmotic flow of a PTT (aqueous ionic solution) fluid through a two-dimensional channel of finite length (L) and uniform thickness of ($2a$), with wavelength λ and wave speed C. The Cartesian coordinate system (x, y) is used in such a way that propagation of the wave is along the x-axis, and the y-axis is considered perpendicular to the direction of the flow. Motion is generated due to propagation of an infinite wave train travelling along the channel wall with speed C. The electro-osmotic flow occurs by the applied external electric field E_x that flows parallel to the channel walls. As a result, the channel experiences electro-osmotic flow as the positive (cations) and negative (anions) ions form the EDL.

The simulation involves the geometry of deforming channel walls:

$$h(\bar{x}, \bar{t}) = a + b\sin\left(\frac{2\pi}{\lambda}(\bar{X} - C\bar{t})\right). \tag{3.1}$$

Here, *b, C, a* and *t* stand for wave amplitude, wave velocity, half-width of the channel and time, respectively.
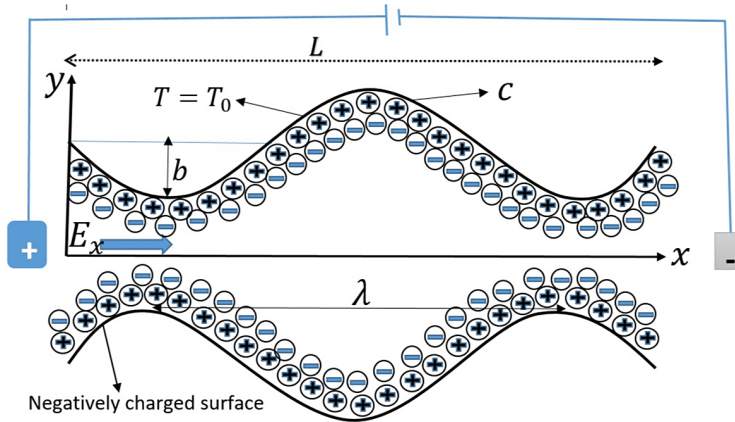
FIGURE 1. Geometry of the problem.

The motion is unsteady because of the moving boundary in the stationary frame $(\bar{X}, \bar{Y})$. However, it can be viewed as steady in the moving frame $(\bar{x}, \bar{y})$. As a result, we can represent the transformations between the fixed and wave frames:

$$\bar{x} = \bar{X} - C\bar{t}, \quad \bar{y} = \bar{Y}, \quad \bar{u}(\bar{x}, \bar{y}) = \bar{U} - C, \quad \bar{v}(\bar{x}, \bar{y}) = \bar{v}, \quad \bar{p}(\bar{x}) = \bar{P}(\bar{X}, \bar{t}).$$

The fundamental equations of continuity, momentum equations with temperature and thermal radiation may be constructed in accordance with the aforementioned [16, 39].

The equations, which can govern the present flow circumstances, are as follows:

$$\frac{\partial \bar{u}}{\partial \bar{x}} + \frac{\partial \bar{v}}{\partial \bar{y}} = 0, \tag{3.2}$$

$$\rho\left(\bar{u}\frac{\partial \bar{u}}{\partial \bar{x}} + \bar{v}\frac{\partial \bar{u}}{\partial \bar{y}}\right) = -\frac{\partial \bar{p}}{\partial \bar{x}} + \frac{\partial \bar{\tau}_{xx}}{\partial \bar{x}} + \frac{\partial \bar{\tau}_{xy}}{\partial \bar{y}} + \bar{\rho}_e \bar{E}_x, \tag{3.3}$$

$$\rho\left(\bar{u}\frac{\partial \bar{v}}{\partial \bar{x}} + \bar{v}\frac{\partial \bar{v}}{\partial \bar{y}}\right) = -\frac{\partial \bar{p}}{\partial \bar{y}} + \frac{\partial \bar{\tau}_{yx}}{\partial \bar{x}} + \frac{\partial \bar{\tau}_{yy}}{\partial \bar{y}} + \bar{\rho}_e \bar{E}_y, \tag{3.4}$$

$$\rho c_p\left(\bar{u}\frac{\partial \bar{T}}{\partial \bar{x}} + \bar{v}\frac{\partial \bar{T}}{\partial \bar{y}}\right) = k\left(\frac{\partial^2 \bar{T}}{\partial \bar{x}^2} + \frac{\partial^2 \bar{T}}{\partial \bar{y}^2}\right) + \bar{\tau}_{xx}\frac{\partial \bar{u}}{\partial \bar{x}} + \bar{\tau}_{yy}\frac{\partial \bar{v}}{\partial \bar{y}} + \bar{\tau}_{xy}\left(\frac{\partial \bar{u}}{\partial \bar{y}} + \frac{\partial \bar{v}}{\partial \bar{x}}\right) + \frac{\partial}{\partial \bar{y}}(\bar{q}_r), \tag{3.5}$$

$$f\bar{\tau}_{xx} + k\left(\bar{u}\frac{\partial \bar{\tau}_{xx}}{\partial \bar{x}} + \bar{v}\frac{\partial \bar{\tau}_{xx}}{\partial \bar{y}} - 2\frac{\partial \bar{u}}{\partial \bar{x}}\bar{\tau}_{xx} - 2\frac{\partial \bar{u}}{\partial \bar{y}}\bar{\tau}_{xy}\right) = 2\mu\frac{\partial \bar{u}}{\partial \bar{x}}, \tag{3.6}$$

$$f\bar{\tau}_{yy} + k\left(\bar{u}\frac{\partial \bar{\tau}_{yy}}{\partial \bar{x}} + \bar{v}\frac{\partial \bar{\tau}_{yy}}{\partial \bar{y}} - 2\frac{\partial \bar{v}}{\partial \bar{x}}\bar{\tau}_{yx} - 2\frac{\partial \bar{v}}{\partial \bar{y}}\bar{\tau}_{yy}\right) = 2\mu\frac{\partial \bar{u}}{\partial \bar{y}}, \tag{3.7}$$

$$f\bar{\tau}_{zz} + k\left(\bar{u}\frac{\partial \bar{\tau}_{zz}}{\partial \bar{x}} + \bar{v}\frac{\partial \bar{\tau}_{zz}}{\partial \bar{y}}\right) = 0, \tag{3.8}$$

$$f\bar{\tau}_{xy} + k\left(\bar{u}\frac{\partial\bar{\tau}_{xy}}{\partial\bar{x}} + \bar{v}\frac{\partial\bar{\tau}_{xy}}{\partial\bar{y}} - \frac{\partial\bar{v}}{\partial\bar{x}}\bar{\tau}_{xx} - \frac{\partial\bar{u}}{\partial\bar{x}}\bar{\tau}_{xy} - \frac{\partial\bar{u}}{\partial\bar{y}}\bar{\tau}_{yy}\right) = \mu\left(\frac{\partial\bar{u}}{\partial\bar{y}} + \frac{\partial\bar{v}}{\partial\bar{x}}\right), \quad (3.9)$$

$$f = 1 + \frac{\epsilon k}{\mu}(\bar{\tau}_{xx} + \bar{\tau}_{yy} + \bar{\tau}_{zz}). \quad (3.10)$$

Here, $\bar{\rho}_e\bar{E}_x$ represents the electro-kinetic body force, $\bar{p}$ represents the pressure, ϵ is the PTT fluid parameter, $\bar{\tau}$ is the stress tensor, $\bar{T}$ is the temperature, k denotes the thermal conductivity, $\bar{u}, \bar{v}$ are the respective velocity components in the radial y- and axial x-directions, c_p is the specific heat constant at pressure, μ is the viscosity, and ρ is the density of the fluid.

Using Rosseland's approximation [39], the radiative heat flux (q_r) is defined as

$$q_r = \frac{-4\bar{\sigma}}{3\bar{k}}\frac{\partial\bar{T}^*}{\partial\bar{y}} \quad \text{and} \quad q = -\kappa\nabla T. \quad (3.11)$$

Here σ, k and q stand for the Stefan–Boltzman constant, thermal conductivity and vector of local heat flux, respectively. We also suppose that the temperature of the fluid within the flow region is sufficiently small. By expanding T^4 about T_0 and ignoring the higher order term obtained,

$$T_0^4 = 4T_0^3 T - 3T_0^4, \quad (3.12)$$

and the above appearance and equation (3.11) now yield

$$q_r = -\frac{16\sigma\bar{T}^3}{3\kappa\mu c_f}\frac{\partial\bar{T}}{\partial\bar{y}}. \quad (3.13)$$

From the Gauss law,

$$\nabla.\bar{E} = \frac{\bar{\rho}_e}{\epsilon}, \quad (3.14)$$

where

$$\bar{E} = -\nabla\Phi. \quad (3.15)$$

Using equation (3.14) in equation (3.15) gives the equation for electrical potential distribution as

$$\nabla^2\Phi = -\frac{\bar{\rho}_e}{\epsilon}, \quad (3.16)$$

in which $\bar{\rho}_e$ and ϵ are the density of the total ionic energy and electric permittivity, respectively. The ions and counter-ions have the equal charge valance $z_+ = z_- = z$ for a symmetric electrolyte.

Thus, the total density of the ionic charge is given by

$$\bar{\rho}_e = ez(\bar{n}_+ - \bar{n}_-), \quad (3.17)$$

where e and z stands for elementary charge and charge balance, respectively. The cations (positive) $\bar{n}_+$ and anions (negative) $\bar{n}_-$ have bulk concentration (number

density). The charge number density must be determined to establish the potential distribution. The Nernst–Plank equation is used to define the distribution of ions inside the fluid as given by Tripathi et al. [38]:

$$\frac{\partial \bar{n}_\pm}{\partial \bar{t}} + \bar{u}\frac{\partial \bar{n}_\pm}{\partial \bar{x}} + \bar{v}\frac{\partial \bar{n}_\pm}{\partial \bar{y}} = \mathbf{D}\left(\frac{\partial^2 \bar{n}_\pm}{\partial \bar{x}^2} + \bar{v}\frac{\partial^2 \bar{n}_\pm}{\partial \bar{y}^2}\right) \pm \frac{\mathbf{D}ez}{T_e K_B}\left[\frac{\partial}{\partial \bar{x}}\left(\bar{n}_\pm \frac{\partial \bar{\Phi}}{\partial \bar{x}}\right) + \frac{\partial}{\partial \bar{y}}\left(\bar{n}_\pm \frac{\partial \bar{\Phi}}{\partial \bar{y}}\right)\right]. \quad (3.18)$$

Here it is presumed that for both species, the ionic diffusion coefficients are equal and that the mobility of the species is determined by the Einstein formula where $\mathbf{D}$ is the diffusion coefficient, K_B is the Boltzmann constant and T_e is the average temperature of the electrolytic solution.

Equation (3.16) is determined as follows in this limit:

$$\frac{\partial^2 \Phi}{\partial y^2} = -m^2\left(\frac{n_+ - n_-}{2}\right), \quad (3.19)$$

where $m = aez\sqrt{2n_0/\epsilon K_B T_e} = a/\lambda_d$ is known as the Debye–Hückel parameter [16], λ_d is the EDL or the Debye length. Additionally, the simplified Nernst–Planck equations are intended to provide the ionic distribution:

$$\frac{\partial^2 n_+}{\partial y^2} \pm \frac{\partial}{\partial y}\left(n_\pm \frac{\partial \Phi}{\partial y}\right) = 0. \quad (3.20)$$

Equation (3.20) with bulk $n_\pm = 1$ at $\Phi = 0$, $\partial n_\pm/\partial y = 0$ at $\partial \Phi/\partial y = 0$, yields the Boltzmann distribution for the ions:

$$n_\pm = e^{\pm \Phi}. \quad (3.21)$$

Substituting equation (3.21) into equation (3.20), one gets the Poisson–Boltzmann paradigm for calculating the distribution of electrical potentials

$$\frac{\partial^2 \Phi}{\partial y^2} = -m^2 \sinh(\Phi). \quad (3.22)$$

Equation (3.22) has to be simplified to proceed with the analysis further. Under Debye–Hückel's linearization [36] (that is, $\Phi < 25$ mV over a large pH range), $\sinh(\Phi) \approx \Phi$. Consequently, equation (3.22) may be reduced to

$$\frac{\partial^2 \Phi}{\partial y^2} = -m^2\Phi. \quad (3.23)$$

Employing the boundary conditions $\partial \Phi/\partial y = 0$ at $y = 0$, and $\Phi = 1$ at $y = h$ to solve equation (3.23),

$$\Phi = \frac{\cosh(my)}{\cosh(mh)}, \quad (3.24)$$

where the electro-osmotic parameter is denoted by $m = a/\lambda_D$.

The condition in equation (3.1) can be written as

$$h = 1 + \phi \sin(2\pi x). \tag{3.25}$$

We introduce some nondimensional parameters as follows:

$$W_e = \frac{kc}{a}, \ u = \frac{\bar{u}}{C}, \ v = \frac{\bar{v}}{C\delta}, \ x = \frac{\bar{x}}{\lambda}, \ y = \frac{\bar{y}}{a}, \ h = \frac{\bar{h}}{a}, \ \delta = \frac{a}{\lambda}, \ p = \frac{\bar{p}a^2}{\mu c\lambda}, \ \theta = \frac{\bar{T} - \bar{T}_0}{\bar{T}_0},$$

$$n = \frac{\bar{n}}{n_0}, \ t = \frac{C\bar{t}}{\lambda}, \ pr = \frac{\mu c_p}{K}, \ Ec = \frac{C^2}{c_f(\bar{T}_0)}, \ \phi = \frac{b}{C}, \ \tau_{ij} = \frac{a\bar{\tau}_{ij}}{C\mu}, \ U_{hs} = -\frac{\psi \epsilon \bar{E}_x}{\mu C},$$

$$Br = Ecpr, \ Re = \frac{\rho Ca}{\mu}, \ \Phi = \frac{\bar{Z}_e \Phi}{K_B T_e}, \ Rd = -\frac{16\delta \bar{T}^3}{3\kappa \mu c_f},$$

where δ is the wave number, W_e is the Weissenberg number, Re is the Reynolds number, Br is the Brinkmann number, pr is the Prandtl number and U_{hs} is the Helmholtz–Smoluchowsky velocity.

Using the aforementioned nondimensional parameters and in accordance with the assumptions of large wave length ($\delta \ll 1$), low Reynolds number ($Re \ll 1$) and the Debay–Hückel linearization, the fundamental equations (3.3)–(3.10) can be scaled in the form:

$$\frac{\partial p}{\partial x} = \frac{\partial \tau_{xy}}{\partial y} - m^2 U_{hs} \frac{\partial^2 \Phi}{\partial y^2}, \tag{3.26}$$

$$\frac{\partial p}{\partial y} = 0, \tag{3.27}$$

$$f\tau_{xx} = 2W_e \frac{\partial u}{\partial y} \tau_{xy}, \tag{3.28}$$

$$f\tau_{yy} = 0 = f\tau_{zz}, \tag{3.29}$$

$$f\tau_{xy} = W_e \frac{\partial u}{\partial y} \tau_{yy} + \frac{\partial u}{\partial y}, \tag{3.30}$$

and

$$(1 + prRd)\frac{\partial^2 \theta}{\partial y^2} = -Br\tau_{xy} \frac{\partial u}{\partial y}. \tag{3.31}$$

The appropriate nondimensional boundary conditions are

$$\begin{cases} \dfrac{\partial u}{\partial y} = 0, & v = 0 \quad \text{at } y = 0, \\ u = -1, & v = -\dfrac{dh}{dx} \quad \text{at } y = h, \end{cases} \tag{3.32}$$

$$\frac{\partial \theta}{\partial y} = 0 \quad \text{at } y = 0, \quad \text{and} \quad \theta = 1 \quad \text{at } y = h. \tag{3.33}$$

3.1. Volume flow rate In the laboratory frame, the following is the expression of the dimensional volume flow rate:

$$Q = \int_0^{\bar{h}} \bar{U}(\bar{X}, \bar{Y}, \bar{t}) \, d\bar{Y}, \tag{3.34}$$

where $\bar{h} = \bar{h}(\bar{X}, \bar{t})$. In the wave frame of reference, the above equation reduces to

$$q = \int_0^{\bar{h}} u(\bar{x}, \bar{y}) \, dy, \tag{3.35}$$

in which $\bar{h} = \bar{h}(\bar{x})$.

From equations (3.1), (3.34) and (3.35),

$$Q = q + C\bar{h}(x).$$

The time averaged value over a fixed frame $\bar{X}$ is

$$\bar{Q} = \frac{1}{T} \int_0^T Q \, dt,$$

which, after using equation (3.35) and performing integration, leads to

$$\varphi = F + 1,$$

where

$$\varphi = \frac{\bar{Q}}{aC},$$
$$F = \frac{q}{aC} = \int_0^h u \, dy. \tag{3.36}$$

Equation (3.29) reveals that $\tau_{yy} = \tau_{zz} = 0$, and the stress tensors' trace changes to τ_{xx}. Substituting equations (3.23) and (3.24) into equation (3.26), and solving with the boundary conditions $\tau_{xy} = 0$ at $y = 0$ (the line of symmetry),

$$\tau_{xy} = y\frac{dp}{dx} - mU_{hs}\frac{\sinh(my)}{\cosh(hm)}. \tag{3.37}$$

With the aid of equations (3.29) and (3.30), we can write

$$\tau_{xx} = 2\epsilon W_e \tau_{xy}^3.$$

From equations (3.10), (3.29) and (3.30),

$$\frac{\partial u}{\partial y} = \tau_{xy} + 2\epsilon W_e^2 \tau_{xy}^3. \tag{3.38}$$

Substituting equation (3.37) into equation (3.38),

$$\frac{\partial u}{\partial y} = y\frac{dp}{dx} - mU_{hs}\frac{\sinh(my)}{\cosh(hm)} + 2\epsilon W_e^2\left(y\frac{dp}{dx} - \frac{mU_{hs}\sinh(my)}{\cosh(hm)}\right)^3. \tag{3.39}$$

4. Analytical solutions

Employing the boundary conditions in equation (3.32) to solve equation (3.39),

$$u = \frac{1}{12}\left[6\left\{-2 - h^2\frac{dp}{dx} + \frac{dp}{dx}y^2 + \left(\frac{dp}{dx}\right)^3(y^4 - h^4)\epsilon W_e\right\} + L_1 + L_2 + L_3\right]. \qquad (4.1)$$

Using equation (3.36) in equation (4.1),

$$F = -h - \frac{h^3}{3}\frac{dp}{dx} - \frac{2}{5}h^5\left(\frac{dp}{dx}\right)^3\epsilon W_e + \frac{U_{hs}}{36m^3}[36m^2(hm - \tanh(hm)) + L_4 + L_5 + L_6]. \qquad (4.2)$$

Due to nonlinearity, it is difficult to obtain the analytical solution to equation (4.2). As a result, the solution is obtained using the standard perturbation approach. We expand dp/dx in terms of the parameter $(|W_e|)$ to use the perturbation approach as follows:

$$\frac{dp}{dx} = p_0 + W_e p_1. \qquad (4.3)$$

The solution of equation (4.2) using equation (4.3) is given by

$$\begin{aligned}
\frac{dp}{dx} = {} & \frac{1}{30h^9m^5}[-90h^6m^5(F + h) + U_{hs}(\tanh(hm) - hm)] + \epsilon W_e(972h^2(F + h)^3m^5) \\
& + L_7 - L_8 + L_9 + L_{10} + L_{11} \\
& + (29160 + 13608h^2m^2 + 405h^4m^4 - 130h^6m^6)\tanh(hm),
\end{aligned} \qquad (4.4)$$

where

$$\begin{aligned}
L_1 = {} & U_{hs}\left[12 - 12\frac{\cosh(my)}{\cosh(hm)} + \frac{\epsilon}{m^2}\left\{72\left(\frac{dp}{dx}\right)^2\left(2 + h^2m^2 - \left\{(2 + m^2y^2)\cosh(my)\right.\right.\right.\right. \\
& \left.\left.\left.\left. + 2m(h\sinh(hm) - y\sinh(my))\right\}\frac{1}{\cosh hm}\right)\right\}\right],
\end{aligned}$$

$$L_2 = 9m^2\frac{dp}{dx}[\cosh(2hm) + 2m\{m(h^2 - y^2) - h\sinh(2hm) + y\sinh(2my)\}]\frac{U_{hs}}{\cosh^2(hm)},$$

$$L_3 = 2m^4[\cosh(3hm) - 9\cosh(hm) + 9\cosh(my) - \cosh(3my)]\frac{U_{hs}^2 W_e}{\cosh(hm)},$$

$$L_4 = \epsilon W_e\left[9m^2\frac{dp}{dx}\{4h^3m^3 + 6hm\cosh(2hm) - 3(1 + 2h^2m^2)\sinh(2hm)\}\frac{U_{hs}}{\cosh^2(hm)}\right],$$

$$L_5 = 2m^4[3hm\cosh(3hm) - 27hm\cosh(hm) + 27\sinh(hm) - \sinh(3hm)]\frac{U_{hs}^2}{\cosh^3(hm)},$$

$$L_6 = 216\left(\frac{dp}{dx}\right)^2[hm(6 + h^2m^2) - 3(2 + h^2m^2)\tanh(hm)],$$

$$L_7 = 1944(F + h)^2m^2U_{hs}(hm(15 + m^2h^2) - 3(5 + 2h^2m^2)\tanh(hm),$$

$$L_8 = 27(F + h)mU_{hs}^2\Big[6h^2m^2(360 + 47m^2h^2) + (2h^2m^2 - 3)\frac{5h^4m^4}{\cosh^2(hm)}$$
$$- 3hm(1440 + 413h^2m^2 + 10h^4m^4)\tanh(hm)\Big],$$

$$L_9 = 108(20 + 9h^2m^2)\tanh(hm)^2,$$

$$L_{10} = U_{hs}^3[87480hm + 60669h^3m^3 + 5508h^5m^5 + 60h^7m^7 - 29160 + 101088h^2m^2$$
$$+ 22599h^4m^4 + 830h^6m^6]\tanh(hm),$$

$$L_{11} = \frac{9hm(-9720 - 3501h^2m^2 - 135h^4m^4 + 10h^6m^6)}{\cosh^2(hm)}.$$

The results shown above are in line with the findings of Hayat et al. [16] when m and U_{hs} approach zero.

The solution for temperature is obtained by solving equation (3.31) with equation (4.1) and boundary conditions in equation (3.33),

$$\theta = \frac{1}{1080m^4(1 + prRd)}\Big[90m^4\Big(12(1 + prRd) + Br\Big(\frac{dp}{dx}\Big)^2(h^4 - y^4)\Big)$$
$$+ Br\frac{dp}{dx}\Big\{72m^4\Big(\frac{dp}{dx}\Big)^3(h^6 - y^6)\epsilon W_e + 135m^2\frac{dp}{dx}\epsilon\Big((9 + 6h^2m^2)\frac{\cosh(2hm)}{\cosh^2(hm)}$$
$$- 3(3 + 2m^2y^2)\cosh(2my) + 2m(m^3(y^4 - h^4) - 6h\sinh(2hm) + 6y\sinh(2my))\Big)U_{hs}^2W_e$$
$$- 20m^4\epsilon\Big(162\cosh(hm) - 2\cosh(3hm) - 162\cosh(my) + 2\cosh(3my)$$
$$+ 3m\{-27h\sinh(hm) + h\sinh(3hm) + 27y\sinh(my) - y\sinh(3my)\}\Big)\frac{U_{hs}^3W_e}{\cosh^3(hm)}$$
$$+ 1080U_{hs}\Big(m^2\{2 + (-2\cosh(my) - hm\sinh(hm))\} + \frac{my\sinh(my)}{\cosh(hm)}$$
$$+ 6\Big(\frac{dp}{dx}\Big)^2\epsilon\Big\{6(4 + h^2m^2)\cosh(hm) - 6(4 + m^2y^2)\cosh(my)$$
$$- hm(18 + h^2m^2)\sinh(hm) + my(18 + m^2y^2)\sinh(my)\Big\}\frac{W_e}{\cosh(hm)}\Big)\Big\}\Big].$$

From equation (4.4), the pressure difference over one wavelength is computed as

$$\Delta p = \int_0^1 \frac{\partial p}{\partial x}\,dx.$$

We now introduce the stream function Ψ as

$$u = \frac{\partial \Psi}{\partial y}, \quad v = -\frac{\partial \Psi}{\partial x}.$$

5. Numerical results and discussion

In this section, we visually display the exact solutions that were computed in the previous section. This allows us to examine the effects of various influential parameters on the flow profile, such as Weissenberg number (W_e), PTT parameter (ϵ), Helmholtz–Smoluchowski velocity (U_{hs}), electro-osmotic parameter (m), thermal radiation parameter (Rd) and Prandtl number (pr). These parameters affect the temperature profile, velocity profile and pressure gradient.

The graphical plots in this section demonstrate the validity of the mathematical solutions and enable a more detailed analysis of the current work. Specifically, the velocity and temperature profiles clearly show that the boundary conditions we used in our situation were valid. The calculated mathematical solutions satisfy the accompanying equations and pertinent boundary conditions. It is worth noting that the axial velocity profiles exhibit a parabolic shape, which is a typical characteristic of no-slip flow. In this type of flow, the velocity is zero at the walls and reaches its maximum in the centre of the microchannel.

Figures 2(a)–(e) depict the analysis of velocity behaviour for different physical parameters in the obtained results. Figure 2(a) illustrates the velocity distributions for the Weissenberg number (W_e). It is evident that higher values of W_e lead to a substantial decrease in fluid velocity. This phenomenon occurs because it assesses the relaxation time of the fluid in relation to a specific process time. As a result, the Weissenberg number decreases the velocity of the fluid while simultaneously increasing its thickness. From Figure 2(b), it is evident that the velocity of the PTT liquid model is directly proportional to the mean flow rate, F. The graph clearly shows that as the intensity of the elastic force, F, increases, the velocity of the fluid also increases. Figure 2(c) is plotted to observe the effect of the parameter ϵ (which represents the extensibility of the fluid) on the velocity field. This graph indicates that the velocity, u, decreases as the value of ϵ increases. Figure 2(d) illustrates that an increase in the electro-osmotic parameter, m, reduces the amplitude of fluid velocity at the centre of the channel ($y = 0$). The electro-osmotic parameter demonstrates that the velocity profile acts as a declining function, although it has a greater influence on fluid velocity. This demonstrates that the electric field enforced along the length of the channel significantly influences controlled haemodynamics. It is evident that the electric field primarily controls the flow in this scenario, and by increasing the electro-kinetic parameter, m, we can regulate the speed of the fluid. This trend is caused by the presence of the electric double layer, which inhibits fluid flow. The argument against the Helmholtz–Smoluchowski parameter based on velocity is illustrated in Figure 2(e). It demonstrates that an increase in U_{hs} velocity leads to a decrease. Therefore, the main purpose of the axial electric field is to control the flow. When $U_{hs} = 0$, there is no electro-osmosis happening during the peristaltic motion of the PTT fluid. The fluid velocity decreases as the EDL thickness increases due to the physical determination of U_{hs}. Consequently, the presence of EDL results in a reduction in fluid flow.
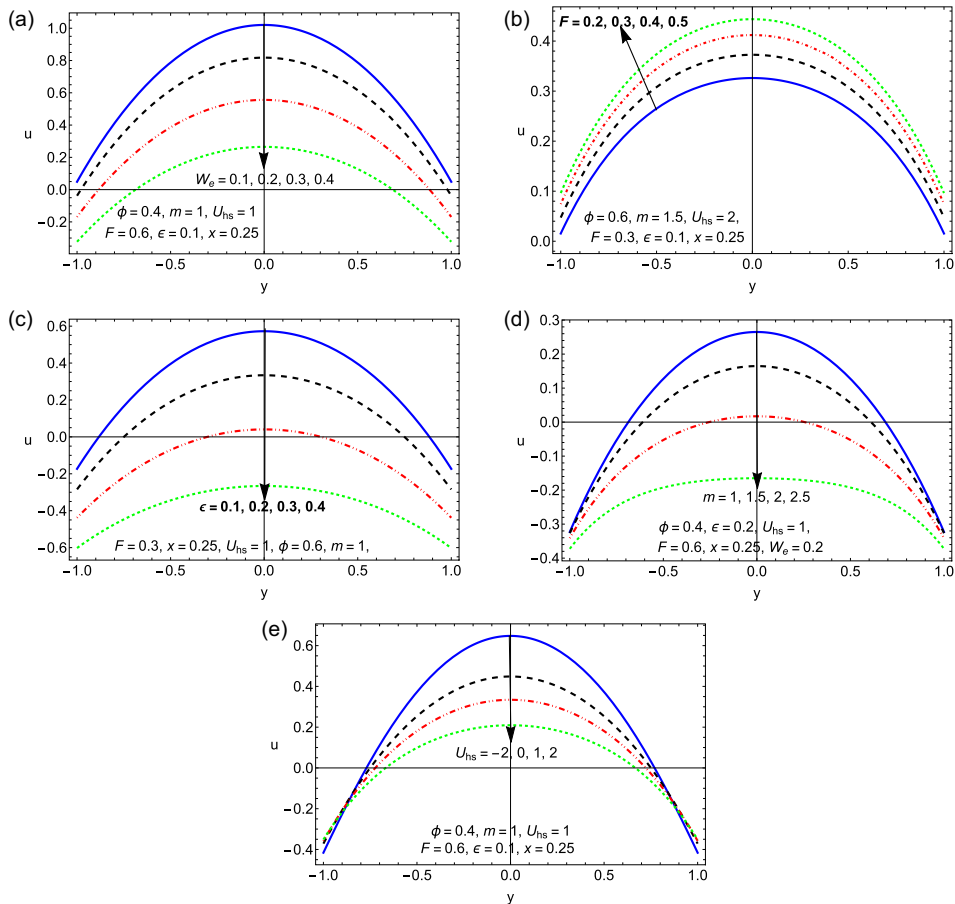
FIGURE 2. Variations of the velocity concerning the y-axis for changed values for (a) Weissenberg number W_e, (b) elastic force (F), (c) PTT parameter (ϵ), (d) electro-osmotic parameter (m) and (e) Helmholtz–Smoluchowski velocity U_{hs}.

To gain insights into the presumed research, we discuss the influence of different constraints on temperature. Figures 3(a)–(f) illustrate the impact of various parameters on temperature distribution. Figure 3(a) depicts the variation in temperature profile with W_e. According to Figure 3(a), it is evident that the temperature reaches its maximum value near the centre of the channel and its minimum value near the walls. This graph clearly shows that when the elastic forces are greater than the viscous forces ($W_e > 1$), the temperature of the liquid significantly decreases. Figure 3(b) demonstrates the effects of increasing the thermal radiation Rd on temperature θ. It is observed that the temperature magnitude decreases as Rd increases. This is due to the inverse relationship between heat radiation and thermal conduction (K). This indicates that when the system's heat radiation is at its highest, the fluid's ability to transmit heat
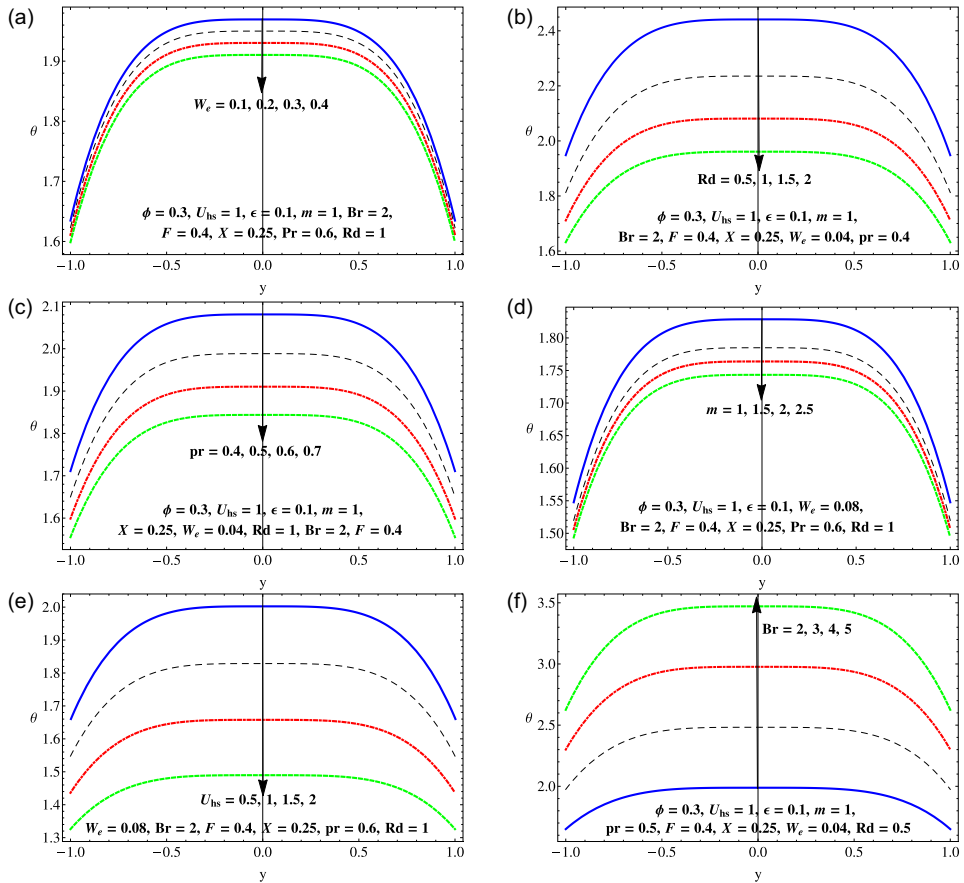
FIGURE 3. Variations of temperature θ concerning the y-axis for changed values for (a) Weissenberg number W_e, (b) thermal radiation Rd, (c) Prandtl number (pr), (d) electroosmotic parameter (m), (e) Helmholtz–Smoluchowski velocity U_{hs} and (f) Brinkman number (Br).

is reduced. Figure 3(c) is plotted to reveal the impacts of Prandtl number pr on heat transfer coefficient. Figure 3(c) indicates that increase in Prandtl number pr slightly decreases the fluid temperature. In Figure 3(d), the electro-osmotic parameter m is plotted against the temperature distribution. The graph shows that as m increases, there is a decline in temperature. This indicates that the relationship between temperature and the electro-kinetic parameter is significant in regulating the heat transfer process. Therefore, it can be concluded that the electric field plays a primary role in controlling heat transmission. Figure 3(e) illustrates that temperature decreases as the values of U_{hs} increase. Specifically, when $U_{hs} = 0.5$, the temperature reaches its highest point and gradually decreases with increasing U_{hs}. This further emphasizes the dependence of temperature on the electric field and its role in regulating heat transport. Figure 3(f) shows the changes in temperature for various values of the Brinkman number Br.
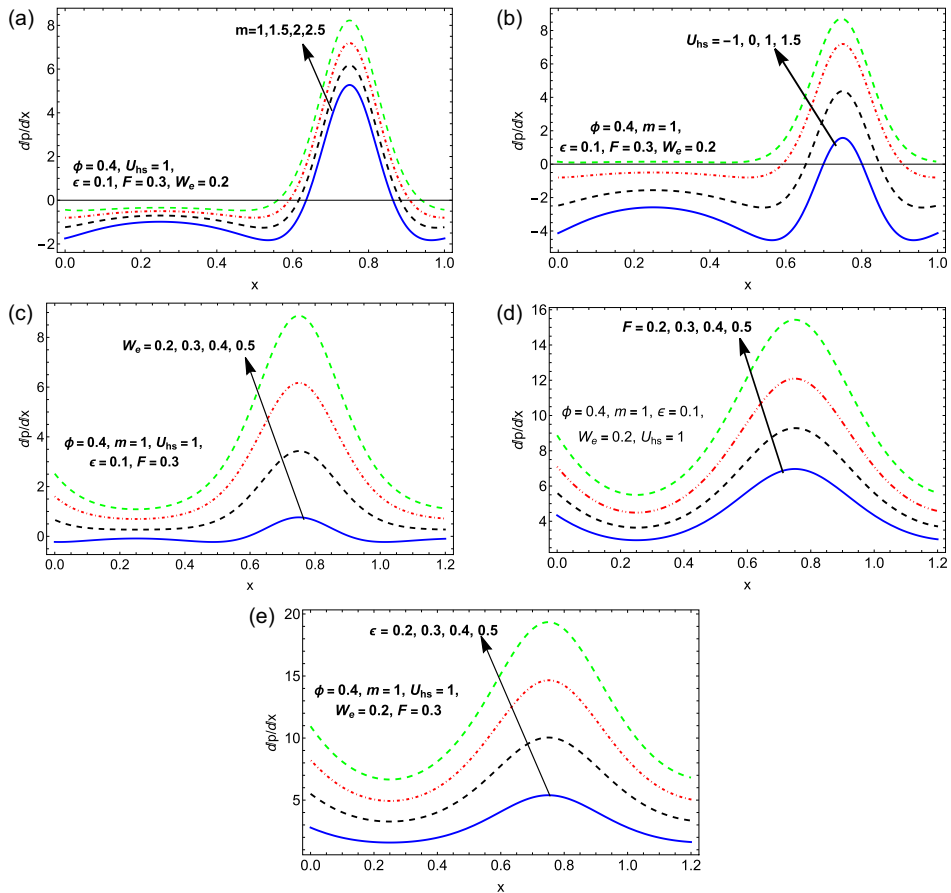
FIGURE 4. Variations of pressure gradient dp/dx concerning the x-axis for changed values for (a) electro-osmotic parameter (m), (b) Helmholtz–Smoluchowski velocity U_{hs}, (c) Weissenberg number W_e, (d) elastic force (F) and (e) PTT parameter (ϵ).

It is demonstrated that the magnitude of the temperature θ increases with an increase in Br. Temperature increases dramatically as a result of this behaviour because a greater magnitude of the Brinkman number means that less heat conduction is produced through viscous dissipation.

Figures 4(a)–(e) demonstrate the impact of various parameters, namely the electro-osmotic parameter (m), Helmholtz–Smoluchowski velocity (U_{hs}), Weissenberg number (W_e), elastic force (F) and PTT parameter (ϵ), on the pressure gradient (dp/dx). It is important to note that the distribution of dp/dx is shown along the axial coordinate (x). The graph clearly shows that the pressure slope along the axial length follows a sinusoidal pattern, with high-pressure gradients during contraction and low-pressure gradients during relaxation. This pattern is crucial in facilitating the peristaltic pumping process. As a result, controlled volume of liquid can be transferred
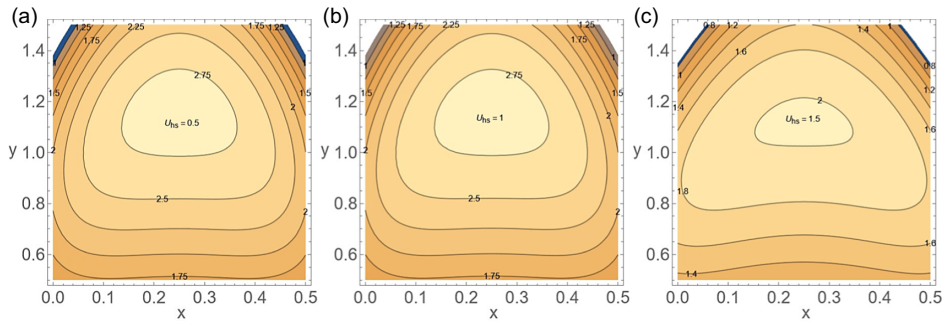
FIGURE 5. Stream lines for $\Phi = 0.3, m = 1, W_e = 0.02, \epsilon = 0.1, F = 0.2$. For (a) $U_{hs} = 0.5$, (b) $U_{hs} = 1.0$ and (c) $U_{hs} = 1.5$.
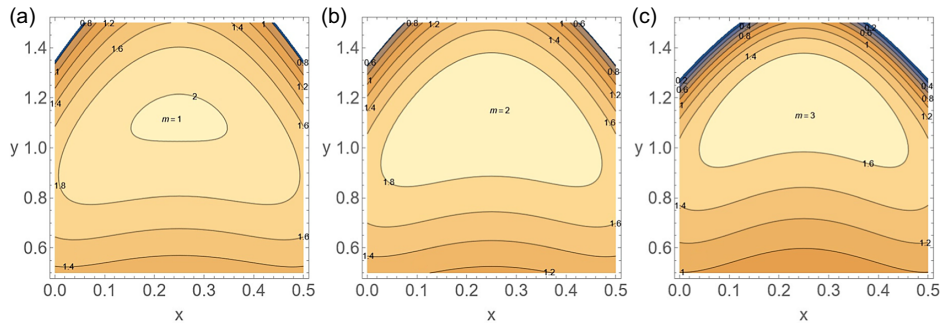

FIGURE 6. Stream lines for $\Phi = 0.3, U_{hs} = 1, W_e = 0.02, \epsilon = 0.1, F = 0.2$. For (a) $m = 1$, (b) $m = 2$ and (c) $m = 3$.

from one area to another without contamination. The pressure gradient for increasing the Debey–Hückel parameter, which is the inverse EDL thickness ($m = a/\lambda_d$), is shown in Figure 4(a). It has been observed that as the Debey–Hückel parameter increases, the pressure gradient also rises. This means that as the typical thickness of the EDL decreases, a negative pressure gradient may occur. Additionally, it is noted that the pressure gradient is insignificant for $x \in [0, 0.6]$ and $x \in [0.9, 1]$, but a large pressure gradient occurs at $x = 0.8$. Figure 4(b) illustrates the variation of dp/dx for different values of the Helmhotz–Smoluchowski velocity (U_{hs}). The pressure gradient consistently increases with an increase in U_{hs}. The electric field in the direction of fluid flow ($U_{hs} > 0$) exhibits the maximum axial pressure gradient compared with the reverse direction of fluid flow ($U_{hs} < 0$). The effect of the rheological parameter W_e on the axial pressure gradient is shown in Figure 4(c). It demonstrates that the axial pressure gradient increases with an increase in the rheological parameter W_e, as there is a direct relationship between dp/dx and the Weissenberg number W_e. The effects of F and ϵ on dp/dx are shown in Figures 4(d) and 4(e). From these graphs, it can be observed that dp/dx increases for large values of F and the PTT fluid parameter ϵ. Furthermore, it is noticed that the maximum pressure gradient occurs at $x = 0.8$.
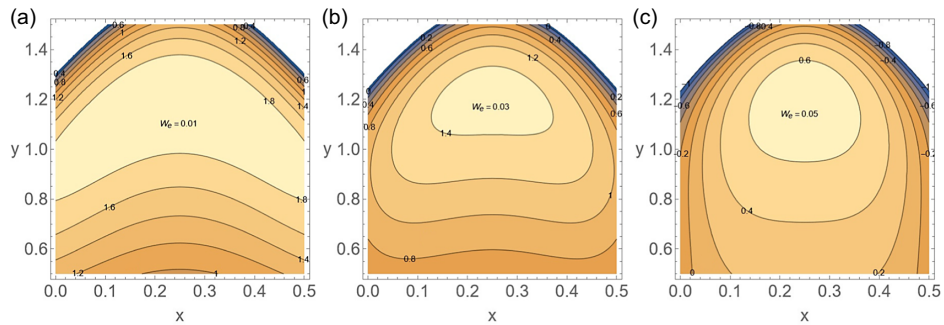
FIGURE 7. Stream lines for $\Phi = 0.3, U_{hs} = 1, m = 1, \epsilon = 0.1, F = 0.2$. (a) $W_e = 0.01$, (b) $W_e = 0.03$ and (c) $W_e = 0.05$.
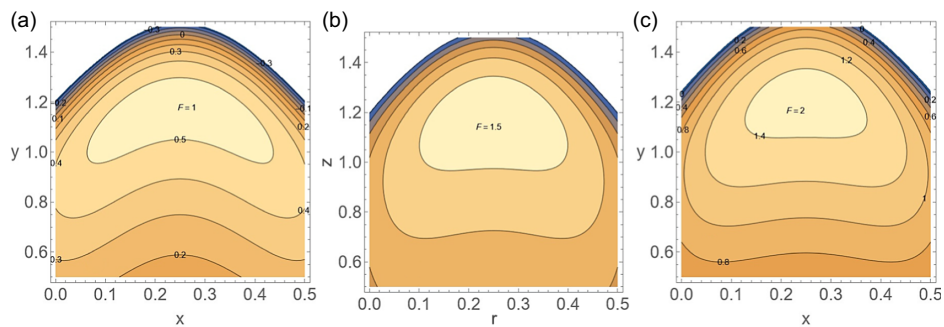

FIGURE 8. Stream lines for $\Phi = 0.3, U_{hs} = 1, m = 1, \epsilon = 0.1, W_e = 0.02$. (a) $F = 1.0$, (b) $F = 1.5$ and (c) $F = 2.0$.

Trapping is significantly important, because it creates a circulatory area that moves forward with the speed of the wave, providing continuous transportation. In the human gastrointestinal tract, smooth muscle tissues contract sequentially to create the peristaltic wave, which propels the food ball (referred to as a bolus in the oesophagus and upper gastrointestinal tract, and chyme in the stomach). This leads to the formation of trapped boluses in confined streamlines. The peristaltic motion of the fluid is shown in Figures 5–8. Figures 5(a)–(c) indicate that the magnitude of the bolus tends to decrease with an increase in the Helmhotz–Smoluchowski parameter U_{hs}. Figures 6(a)–(c) reveal that the size of bolus increases as the Debey–Hückel parameter m increases while the number of boluses is decreasing. Figures 7(a)–(c) conclude that the extent of the trapped bolus is increased with a rise in the parameter W_e. Figures 8(a)–(c) display the effect of different values of the PTT liquid parameter F on the streamlines. It shows that an increase in F leads to a decrease in the size of the trapped bolus, while only slightly increasing the number of streamlines in the top symmetric micro-channel.

6. Conclusions

To improve the understanding of the peristaltic motion of PTT fluids, this study introduces additional factors such as electro-osmosis, thermal radiation and heat transfer in the planar micro-channel. These findings can be used to optimize the operation of bio-microfluidic devices that use electro-osmosis and peristalsis. The problem at hand has been solved analytically, providing solutions for the velocity, temperature and pressure gradient of the fluid model under consideration. Graphical representations have been used to illustrate their physical behaviour. The main outcomes of this study are as follows.

- The velocity reaches its highest value in the core of the channel and is directly related to the Weissenberg number.
- The velocity decreases as the Helmhotz–Smoluchowski parameter (U_{hs}) increases.
- An increase in the PTT fluid parameter (ϵ) leads to an increase in velocity.
- The Debye–Hückel parameter greatly enhances the temperature field at the centre of the channel.
- The temperature profile decreases with an increase in the Prandtl number (pr) and thermal radiation (Rd) number.
- The pressure gradient increases for larger values of the Weissenberg number (W_e), elastic parameter (F) and PTT fluid parameter (ϵ).
- The size and number of boluses decrease with an increase in the Helmhotz–Smoluchowski parameter (U_{hs}).
- An increase in the PTT fluid parameter (ϵ) results in a reduction in the size of trapped boluses, while only slightly increasing the number of streamlines in the top symmetric microchannel.
- As the fluid parameter and electro-osmotic parameter increased, the trapping bolus ultimately disappeared.

Acknowledgement

References

[1]   A. M. Abbas, M. M. Bhatti and M. M. Rashidi, "Peristaltic blood flow of Ellis fluid through a non-uniform channel having compliant walls", *J. Nanofluid* **6** (2019) 318–323; doi:10.1166/jon.2017.1314.

[2]   A. E. H. Abd El Naby, "Creeping flow of Phan–Thien–Tanner fluids in a peristaltic tube with an infinite long wavelength", *ASME J. Appl. Mech.* **76** (2009) Article ID: 064504; doi:10.1115/1.3132183.

[3]   N. S. Akbar, A. Butt, D. Tripathi and O. A. Bég, "Physical hydrodynamic propulsion model study on creeping viscous flow through a ciliated porous tube", *Pramana – J. Phys.* **88** (2017) 1–9; doi:10.1007/s12043-016-1354-z.

[4] S. Akhtar, L. B. McCash, S. Nadeem, S. Saleem and A. Issakhov, "Mechanics of non-Newtonian blood flow in an artery having multiple stenosis and electroosmotic effects", *Sci. Prog.* **104** (2021) 1–15; doi:10.1177/00368504211031693.

[5] H. Ashraf, A. M. Siddiqui and M. A. Rana, "Fallopian tube analysis of the peristaltic-ciliary flow of third grade fluid in a finite narrow tube", *Chinese J. Phys.* **56** (2018) 605–621; doi:10.1016/j.cjph.2018.02.001.

[6] A. Bandopadhyay, D. Tripathi and S. Chakraborty, "Electro-osmosis-modulated peristaltic transport in microfluidic channel", *Phys. Fluids* **28** (2016) Article ID: 052002; doi:10.1063/1.4947115.

[7] A. W. Butt, N. S. Akabar and N. A. Mir, "Heat transfer analysis of peristaltic flow of a Phan–Thien–Tanner fluid model due to metachronal wave of cilia", *Biomech. Model. Mechanobiol.* **19** (2020) 1925–1933; doi:10.1007/s10237-020-01317-4.

[8] A. W. Butt, N. S. Akbar, R. Mehmood and S. Farooq, "Thermally conductive electro-osmotic propulsive pressure-driven peristaltic streaming flow study with a suspended nanomaterial in a micro-ciliated tube", *Front. Mater.* **9** (2022) 1–11; doi:10.3389/fmats.2022.1059816.

[9] S. Chakraborty, "Augmentation of peristaltic micro flows through electro-osmotic mechanisms", *J. Phys. D* **39** (2006) Article ID: 5356; doi:10.1088/0022-3727/39/24/037.

[10] M. M. Channakote and S. K. Asha, "Heat transfer and electro-osmotic analysis on peristaltic pumping of a fractional second-grade fluid through a cylindrical tube", *Int. J. Comput. Mat. Sci. Eng.* **12** (2023) Article ID: 2350007; doi:10.1142/S2047684123500070.

[11] M. M. Channakote and D. V. Kalse, "Heat transfer in peristaltic motion of Rabinowitsch fluid in a channel with permeable wall", *Appl. Appl. Math.* **16** (2021) 1–19; https://digitalcommons.pvamu.edu/aam/vol16/iss2/16/.

[12] M. M. Channakote and D. V. Kalse, "Combined convective and viscous dissipation effects on peristaltic flow of Ellis fluid in a non-uniform tube", *J. Naval Arch. Marine Eng.* **19** (2022) 1–20; doi:10.3329/jname.v19i1.55052.

[13] P. Goswami, P. K. Mondal, A. Datta and S. Chakraborty, "Entropy generation minimization in an electroosmotic flow of non-Newtonian fluid: effect of conjugate heat transfer", *ASME J. Heat Transf.* **138** (2016) Article ID: 051704; doi:10.1115/1.4032431.

[14] P. Gravesen, J. Branebjerg and O. S. Jensen, "Microfluidics-a review", *J. Micromech. Microeng.* **3** (1993) 168–174; doi:10.1088/0960-1317/3/4/002.

[15] S. J. Haswell, "Development and operating characteristics of micro flow injection based on electroosmotic flow", *Analyst* **122** (1997) 1R–10R; doi: 10.1039/A606289J.

[16] T. Hayat, S. Noreen, N. Ali and S. Abbasbandany, "Peristaltic motion of Phan–Thien–Tanner fluid in a planner channel", *Numer. Methods Partial Differential Equations* **28** (2010) 737–748; doi:10.1002/num.20647.

[17] T. Hayat, S. Rani, A. Alsaedi and M. Rafiq, "Radiative peristaltic flow of magneto nanofluid in a porous channel with thermal radiation", *Results Phys.* **7** (2017) 3396–3407; doi:10.1016/j.rinp.2017.07.074.

[18] X. Huang, M. J. Gordon and R. N. Zare, "Current–monitoring method for measuring the electroosmotic flow rate in capillary zone electrophoresis", *Anal. Chem.* **60** (1998) 1837–1838; doi:10.1021/ac00168a040.

[19] S. Hussain, N. Ali and K. Ullah, "Peristaltic flow of Phan–Thien–Tanner fluid: effects of peripheral layer and electroosmotic force", *Rheol. Acta.* **58** (2019) 603–618; doi:10.1007/s00397-019-01158-8.

[20] Y. Kang, C. Yang and X. Huang, "Electroosmotic flow in a capillary annulus with high zeta potentials", *J. Colloid Interface Sci.* **253** (2002) 285–294; doi:10.1006/jcis.2002.8453.

[21] M. Kothandapani and J. Prakash, "Effects of thermal radiation parameter and magnetic field on the peristaltic motion of Williamson nano fluids in a tapered asymmetric channel", *Int. J. Heat Mass Transf.* **81** (2015) 234–245; doi:10.1016/j.ijheatmasstransfer.2014.09.062.

[22] T. W. Latham, "Fluid motion in a peristaltic pump", Master's Thesis, Massachusetts Institute of Technology, Cambridge, 1966. https://dspace.mit.edu/handle/1721.1/17282.

[23] M. C. Mahadev and A. Mohanta, "Thermal radiation effect on Phan–Thien–Tanner liquid model obeying peristaltic activity with cilia waves", *World Sci. News* **183** (2023) 210–226; https://worldscientificnews.com/wp-content/uploads/2024/01/WSN-183-2023-210-226.pdf.

[24] J. C. Misra, G. C. Shit, S. Chandra and P. K. Kundu, "Electro-osmotic flow of a viscoelastic fluid in a channel: applications to physiological fluid mechanics", *Appl. Math. Comput.* **217** (2011) 7932–7939; doi:10.1016/j.amc.2011.02.075.

[25] P. Muthu, B. V. R. Kumar and P. Chandra, "On the influence of wall properties in the peristaltic motion of micro polar fluid", *ANZIAM J.* **45** (2003) 245–260; doi:10.1017/S1446181100013304.

[26] S. Nadeem, A. Riaz, R. Ellahi and N. S. Akbar, "Mathematical model for the peristaltic flow of Jeffrey fluid with nanoparticles phenomenon through a rectangular duct", *Appl. Nano Sci.* **4** (2014) 613–624; doi:10.1007/s13204-013-0238-5.

[27] S. Nadeem and H. Sadaf, "Metachronal wave of cilia transport in a curved channel", *Z. Naturforschung A* **70** (2015) 33–38; doi:10.1515/zna-2014-0117.

[28] S. Noreen, "Pressure driven flow of PTT fluid in a channel with heat transfer and inclined magnetic field", *Int. J. Appl. Comput. Math.* **3**(Suppl. 1) (2017) 1497–1509; doi:10.1007/s40819-017-0423-4.

[29] J. Prakash and D. Tripathi, "Study of EDL phenomenon in peristaltic pumping of a Phan–Thien–Tanner fluid through asymmetric channel", *Korea-Aust. Reh. J.* **32** (2020) 271–285; doi:10.1007/s13367-020-0026-1.

[30] M. Y. Rafiq and Z. Abbas, "Impacts of viscous dissipation and thermal radiation on Rabinowitsch fluid model obeying peristaltic mechanism with wall properties", *Arab. J. Sci. Eng.* **46** (2021) 12155–12163; doi:10.1007/s13369-021-05870-7.

[31] V. P. Rathod and M. Mahadev, "Interaction of heat transfer and peristaltic pumping of fractional second grade fluid through a vertical cylindrical tube", *Therm. Sci.* **18** (2014) 1109–1118; doi: 10.2298/TSCI111022143R.

[32] F. F. Reuss, "Notice sur un nouvel effect de l'électricité galvanique", *Mém. Soc. Imp'ériale Nat. Moscou* **2** (1816) 327–337; https://www.biodiversitylibrary.org/item/234594#page/16/mode/1up.

[33] S. Saleem, S. Akhtar and S. Nadeem, "Mathematical study of electro osmotically driven peristaltic flow of Casson fluid inside a tube having systematically contracting and relaxing sinusoidal heated walls", *Chinese J. Phys.* **71** (2021) 300–311; doi:10.1016/j.cjph.2021.02.015.

[34] S. Saleem, F. Hussain, M. Irfan, I. Siddique, M. Nazeer and S. M. Eldin, "Theoretical investigation of heat transfer analysis in Ellis nanofluid flow through the divergent channel", *Case Stud. Therm. Eng.* **48** (2023) Article ID: 103140; doi:10.1016/j.csite.2023.103140.

[35] G. Sunitha and S. K. Asha, "Influence of thermal radiation on peristaltic blood flow of a Jeffrey fluid with double diffusion in the presence of gold nano particles", *Inform. Med. Unlocked* **17** (2019) Article ID: 100272; doi:10.1016/j.imu.2019.100272.

[36] D. Tripathi, S. Bushan and O. A. Bég, "Analytical study of electro-osmosis modulated capillary peristaltic hemodynamics", *J. Mech. Med. Biol.* **17** (2017) Article ID: 1750052; doi: 10.1142/S021951941750052X.

[37] D. Tripathi, R. Jhorar, O. A. Bég and S. Shaw, "Electroosmosis modulated peristaltic biorheological flow through an asymmetric microchannel: mathematical model", *Meccanica* **53** (2018) 2079–2090; doi:10.1007/s11012-017-0795-x.

[38] D. Tripathi, A. Sharma, O. A. Bég and A. Tiwari, "Electrothermal transport in biological systems: an analytical approach for electro kinetically modulated peristaltic flow", *ASME J. Therm. Sci. Eng. Appl.* **9** (2017) Article ID: 041010; doi:10.1115/1.4036803.

[39] K. Vajravelu, S. Sreenadh, S. Dhananjaya and P. Lakshminarayana, "Peristaltic flow and heat transfer of a conducting Phan–Thien–Tanner fluid in an asymmetric channel-application to chyme movement in small intestine", *Int. J. Appl. Mech. Eng.* **21** (2016) 713–736; doi:10.1515/ijame-2016-0042.

[40] S. Waheed, S. Noreen and A. Hussanan, "Study of heat and mass transfer in electroosmotic flow of third order fluid through peristaltic microchannels", *Appl. Sci.* **9** (2019) Article ID: 2164; doi:10.3390/app9102164.

[41] W. Zhang, M. He, T. Yuan and W. Xu, "A two-step method for rapid characterization of electroosmotic flows in capillary electrophoresis", *Electrophoresis* **38** (2017) 3130–3135; doi:10.1002/elps.201700215.